Computers and Geotechnics 55 (2014) 342–351

Contents lists available at ScienceDirect

Computers and Geotechnics

journal homepage: www.elsevier.com/locate/compgeo

Discrete element modeling for the study of the effect of soft inclusions on the behavior of soil mix material

G. Van Lysebetten [a,*], A. Vervoort [a], J. Maertens [b], N. Huybrechts [c]

[a] Department of Civil Engineering, KU Leuven, Leuven, Belgium
[b] Jan Maertens BVBA and Department of Civil Engineering, KU Leuven, Leuven, Belgium
[c] Belgian Building Research Institute, Geotechnical Division, Limelette, Belgium

ARTICLE INFO

Article history:
Received 21 January 2013
Received in revised form 26 May 2013
Accepted 29 September 2013

Keywords:
Discrete element method
Numerical simulations
Deep soil mixing
Soft inclusions
Fracturing

ABSTRACT

The influence of soil inclusions on the mechanical behavior of deep soil mix material was studied by discrete element simulations in combination with some laboratory tests. The innovative aspect of the simulations was that individual fracturing in the heterogeneous material was modeled. It was observed that the reduction of strength and stiffness did not correspond to the weighted average of the UCS and Young's modulus, taking into account the volumes of the strong and weak material. The actual reduction was considerably larger, e.g., on average the strength was reduced by 13% and 50% for 1% and 10% of inclusions, respectively. Moreover, other parameters, such as the shape, number, and relative position of inclusions, also have an important influence on the strength and stiffness. First, sharp-ended inclusions have a more negative impact on the strength and stiffness than rounded inclusions. Second, one large inclusion reduces strength and stiffness more than three smaller inclusions with the same shape and accounting for the same total volume percentage. Finally, diagonally-located and more-concentrated inclusions have a more negative impact on the mechanical behavior than vertically-aligned and widely-spread inclusions. The results of the numerical simulations showed good agreement with the results of laboratory tests with regard to the effect on strength and stiffness as well as the observed fracture patterns.

1. Introduction

1.1. Deep soil mixing technique

The deep soil-mixing technique has been used for ground improvement applications for several decades [1]. Currently, it is being used increasingly for the construction of soil- and water-retaining structures because of its economical and environmental advantages compared with classical techniques, such as concrete secant pile walls, diaphragm walls, and king post walls (i.e., soldier pile walls).

The soil-mixing technique is based on an in situ mechanical mixing of the soil with an injected binder (e.g., cement). By executing overlapping rectangular panels or cylindrical columns, a continuous wall is obtained. As soon as the panel or column has been mixed, steel H or I profiles are inserted into the fresh soil mix material to increase the shear and bending resistance of the wall. Depths up to 20 m have been reached.

Because of the specific mixing procedure of the soil-mixing technique and since a natural material is directly used as building material, the presence of soil inclusions (i.e., unmixed and thus weaker parts) is inevitable. The volume percentage varies between 0% and 3.5% in sandy soils up to 35% and more in stiff clays [2]. Apart from this, soil inclusions can be very small (a few millimeters), but large inclusions (up to 100–200 mm) also are found. This is illustrated by the two soil-mix cores of Fig. 1a, originating from the same soil-mix panel executed in a sandy soil (with a length of about 550 mm). In the upper core, a large inclusion, with a diameter of about 50 mm, was observed, while the sizes of the inclusions in the lower core were limited to a few millimeters. Note that both the inclusions, the execution parameters (e.g., amount of binder injected, water/cement ratio), and the type of soil influence the Uniaxial Compressive Strength (UCS) value. All of these factors can lead to a wide range of UCS values on one construction site, as illustrated by Fig. 1b, which shows the histogram of 31 UCS values for a Belgian construction site in a loamy soil.

1.2. Need for alternative design rules

The heterogeneous nature of soil-mix material precludes the application of classical design rules because they are valid only for homogeneous building materials. Moreover, the statistical

* Corresponding author. Present address: Belgian Building Research Institute, Geotechnical Division, Avenue P. Holoffe 21, B-1342 Limelette, Belgium. Tel.: +32 2 655 77 74; fax: +32 2 653 07 29.
E-mail addresses: gvl@bbri.be (G. Van Lysebetten), andre.vervoort@bwk.kuleuven.be (A. Vervoort), jan.maertens.bvba@skynet.be (J. Maertens), nh@bbri.be (N. Huybrechts).

0266-352X/$ - see front matter © 2013 Elsevier Ltd. All rights reserved.
http://dx.doi.org/10.1016/j.compgeo.2013.09.023

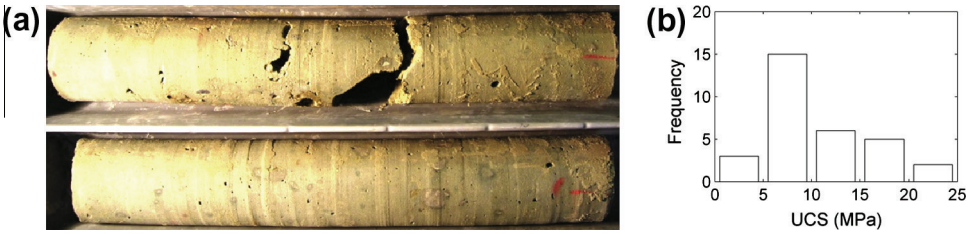

Fig. 1. (a) Two cores with a length of about 550 mm from the same soil-mix panel. The soil in the inclusions was washed out during coring. (b) Histogram of 31 UCS values of soil-mix samples from a construction site in Belgium (loam).

distribution of the UCS values of the soil-mix data is often strongly negatively or positively skewed, instead of being distributed symmetrically, as is assumed by classical design rules (e.g., the histogram in Fig. 1b clearly has a positively-skewed distribution). Classical design rules usually are defined as the mean value minus the standard deviation multiplied by a factor that corresponds to a certain confidence interval. However, this approach often leads to unrealistic characteristic values (i.e., even less than zero), while, in practice, the soil-mix material performs sufficiently well [3].

Therefore, in 2009, the Belgian Building Research Institute (BBRI), the Belgian Association of Foundation Contractors (ABEF), and KU Leuven applied for a project subsidized by the Flemish Government Agency for Innovation by Science and Technology (IWT). The aim of the project was to reformulate the classical design rules to the fundamental behavior of soil-mix material, taking into account the heterogeneous character, soil inclusions, scale effect, and time effects, such as curing time and creep. During the project, attention was paid mainly to the compressive strength of the soil-mix material, the adherence between the soil-mix material and steel reinforcement, and the sustainability and permeability of the material.

Within the scope of this project, a large number of laboratory tests were conducted, but numerical simulations also were conducted, allowing the study of the occurrence and growth of individual fractures in the heterogeneous material during loading. By approximating the failure process of fracture initiation and growth as realistically as possible, the simulations can be used for prediction of new situations, e.g., more or less heterogeneities, larger or smaller heterogeneities, and the scale effect. Apart from the UCS tests on core samples, large soil-mix blocks (600 $\times$ 1200 mm) were tested to study the scale effect [4]. The main focus of this article is the results of the numerical simulations.

2. Discrete element modeling

2.1. Simulation of fracturing

The failure of rock is determined mainly by the initiation and propagation of fractures in the rock material. At relatively low loads, fracturing can be initiated by micro-fractures that develop into macro-fractures at higher loads. The approximations provided by the classical elasto-plastic continuum models are, for the most part, sufficiently accurate to simulate global deformation behavior [5]. However, simulation of fracture initiation and growth is still necessary, e.g., to allow a correct distinction between shear and tensile fractures, but also to understand and quantify the effect of heterogeneities in the material. Several numerical approaches have been developed during the past few decades to simulate crack propagation.

The finite element method (FEM) is a tool that is used extensively in structural analysis [6]. Since it is based on the theory of continuum mechanics, it is not well suited for the analysis of crack propagation. However, discrete as well as continuum numerical approaches have been developed for modeling discontinuities [7]. In the discrete approach, a crack is represented by a real mesh discontinuity [8]. This implementation requires remeshing to cater to crack propagation, which makes the modeling of arbitrary crack growth in FEM very difficult. Several finite element based methods have been proposed without the need of remeshing. However, some of the methods, such as the Element-Free Galerkin (EFG) method [9] and the Element-Free Galerkin Particle (EFG-P) method [10], have encountered difficulties in enforcing essential boundary conditions and numerical integration. In addition, they have high computational expense. More recently, methods referred to as 'partition of unity' (PU) methods have been developed extensively (e.g., the Extended Finite Element Method (XFEM), which incorporates enrichment functions to simulate simple crack propagation [11]). Nevertheless, to deal with more complicated configurations (e.g., the growth of multiple cracks) all these methods still must be improved.

Apart from these and other methods, such as the Finite Difference Method (FDM) and the Displacement Discontinuity Boundary Element Method (DD-BEM) that allow the simulation of fracture growth, the Distinct Element Method (DEM) is a very valuable alternative [12]. The studied domain was divided into a mesh of separate (rigid or deformable) elements, bonded together by contacts. Several DEM codes have been developed. In the Particle Flow Code (PFC), for example, materials are modeled as a dense packing of rigid spherical elements, bonded together at their contact points [13]. For this study, the Universal Distinct Element Code (UDEC) was chosen because it is a familiar, efficient, and reliable software package. Originally, it was developed for the simulation of the behavior of a fractured rock mass, e.g., its slope stability [14]. However, in the past, it has been used successfully for the numerical modeling of fracture initiation and growth in rock [15,16]. The fact that our research group at KU Leuven already had experience with this code certainly was a significant factor in the selection of this particular code.

2.2. Global approach

UDEC is a 2D numerical program that is based on the discrete element method [17]. The discrete elements model consists of discrete blocks that are mutually connected by contacts. Tensile and shear failure criteria are defined for these contacts, allowing them to open and deform upon activation. The UDEC solution scheme is based on a (dynamic) explicit finite-difference method, which also is used in continuum analysis [18]. UDEC was developed to study various phenomena, such as rock fall and slope instability, which depend on the activation of existing fractures. The philosophy followed in this study is that by dividing a medium in multiple discrete small blocks (tightly bound together), their boundaries can act as potential fracture paths when an external load is applied [5,15]. In other words, a contact between two adjacent blocks does not represent a physical crack as long as it is not activated. An example of a mesh of triangles for a rectangular medium is shown

in Fig. 2a. Since fracture growth is limited to the available contacts, the distribution of the contacts should be as uniform as possible so that the mesh does not create any bias. On a larger scale, a given fracture with a certain overall direction tends to develop as a combination of activated individual contacts that sometimes have very different orientations, as illustrated in Figs. 2b and c for a 60° inclined crack.

In this study, the blocks only deform elastically. Thus, the strength parameters of the material are not implemented explicitly in the blocks. However, the contacts are modeled with an elasto-plastic, Mohr–Coulomb, failure criterion with tension cut-off. After activation, the strength parameters are set to residual values. In addition to this, contacts in UDEC are conceptualized as springs and are modeled consequently with two types of stiffness, in the shear and normal directions, k_s and k_n, respectively. This stiffness allows deformation of the contacts prior to activation. The deformation due to the stiffness of the contacts has an effect on the stress distribution within the sample [19].

2.3. Calibration process

Although UDEC is a 2D code, each model, in fact, has a unit thickness. The condition of plane strain was used in all simulations. That is probably the reason that good agreement was observed between the simulations and the results of the laboratory experiments involving the uniaxial compression of cylindrical samples. Therefore, the authors decided to conduct a parametric study using this 2D code, because the complexity of calibration, as well as the run time, increases significantly when a real 3D code is used. Of course, when there is a need, in a later phase, to simulate other loading conditions in the laboratory (e.g., triaxial loading) or the in situ behavior, it will probably be necessary to use a 3D code.

A good calibration is not always straightforward, and various approaches can lead to a satisfactory result. Here, the calibration was based on the ultimate strength and the Young's modulus, but also on the observed fracture pattern, which is feasible when a discrete element code is used. First, the triangular blocks are given material properties that were obtained from laboratory tests (Table 1). Since the stiffness and strength parameters of the contacts are not physically measurable, their values were deduced from a calibration process. The contact properties for a homogeneous model of well-mixed material were calibrated based on the stress-strain behavior and typical fracture patterns (60–70° inclined shear fractures) during uniaxial compression tests. The influence of small changes in the contact parameters on the stress–strain behavior (including strength and stiffness) and the fracture pattern also were studied. This process leads to the (matrix–matrix) contact strength and stiffness parameters presented

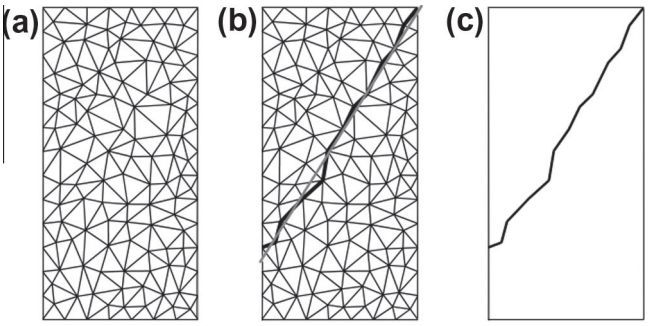

Fig. 2. (a) Simplified example of adjacent triangular blocks that form the sample. A contact only represents a physical crack when it is activated. (b) Fracture along activated contacts with a global dip of 60°. (c) Apart from the activated contacts, the sample is still intact.

Table 1
Material properties of the blocks corresponding to the matrix material and the soft inclusions.

Material properties	Matrix	Inclusions
Density ρ (kg/m^3)	1820	1820
Cohesion (kPa)	3050	5
Tensile strength (kPa)	1500	5
Young's modulus E (GPa)	11.6	0.165
Poisson's ratio υ (–)	0.3	0.4
Bulk modulus K (GPa)	9.67	0.275
Shear modulus G (GPa)	4.46	0.059

in Table 2. The normal and shear contact stiffness are both equal to 65×10^{12} Pa/m, the contact cohesion is equal to 6000 kPa, and the tensile strength of the contacts is equal to 3000 kPa. Note that these contact parameters are the same throughout the homogeneous sample. The whole assembly of contacts leads to a certain strength and stiffness of the sample and also determines the resulting fracture pattern during UCS testing. A sample with these properties results in a UCS value of 11.7 MPa and a Young's modulus of 10.5 GPa; both values are very similar to these observed in laboratory experiments (e.g., the UCS value lies in the range of UCS values of the 31 soil-mix samples presented in Fig. 1b) [1,3].

Next, the strength properties of the contacts between mixed and unmixed material and between both unmixed material, i.e., matrix–inclusion and inclusion–inclusion contacts, were deduced easily from the matrix–matrix contact strength by applying the strength ratios of the mixed and unmixed material. The cohesion and tensile strength of matrix (mixed) material (3050 and 5 kPa, respectively) and unmixed material (1500 and 5 kPa, respectively) were in the proportions of 600/1 and 300/1, respectively. Applying these ratios to the cohesion and tensile strength of the matrix–matrix contact parameters leads to both a cohesion strength and a tensile strength of 10 kPa for the matrix–inclusion and inclusion–inclusion contacts (Table 2). The contact stiffness parameters remain unchanged. As for the homogeneous sample, heterogeneous samples with these contact parameters lead to realistic and representative results, as presented in Section 3.

2.4. Basic model

The starting point for the models of the soil-mix samples is a section through a real soil-mix column in which an area of 120×240 mm is considered (Fig. 3a). This section contains 11 inclusions that account for a surface percentage of 11%. Since, for example, the aim was to use simulations to study the effect of the varying percentage of inclusions, the basic or reference model was based on this real section, but only nine of the 11 inclusions were considered, so that a rounded figure of 10% could be considered for this basic model (Fig. 3b). The shape and position of these nine inclusions were the same as in the real section. For the other models, simple percentages also were considered (i.e., 1%, 5%, 10%, or 20% of inclusions). Even though a 2D model was used, the term vol% is used systematically in the further discussion of the results. In this way, the link with the measurements on the real soil-mix material can be made more easily; the term vol% was considered to be justifiable because the model had a unit thickness.

2.5. Mesh-generation algorithm

As illustrated by the basic model in Fig. 3b, the mesh of a soil-mix sample is built up by a combination of a pre-defined structure and a certain degree of randomness. In other words, the pre-defined shape and location of the inclusions are incorporated in a (random) mesh of triangles. Since UDEC does not provide a mesh

Table 2
Contact properties of the different types of contacts according to the Coulomb slip model, obtained by calibration.

Contact properties	Matrix–matrix	Matrix–inclusion	Inclusion–inclusion
Normal stiffness k_n ($\times 10^{12}$ Pa/m)	65	65	65
Shear stiffness k_s ($\times 10^{12}$ Pa/m)	65	65	65
Cohesion *jcoh* (kPa)	6000	10	10
Tension strength σ_T/*jten* (kPa)	3000	10	10
Friction angle φ (°)	34	34	34
Residual cohesion (kPa)	0	0	0
Residual tension strength (kPa)	0	0	0
Residual friction angle φ_{res} (°)	34	34	34

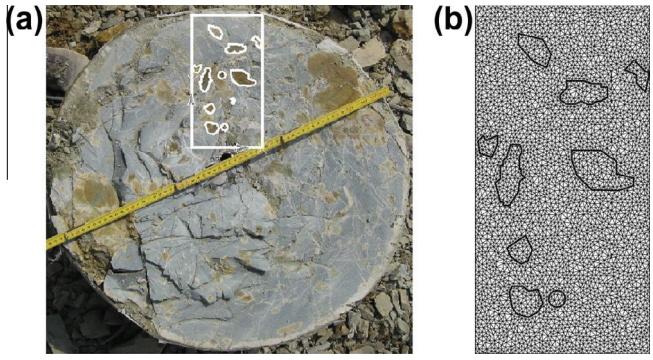

Fig. 3. (a) 2D sample (120 × 240 mm) from the cross section of a real soil-mix column. (b) Mesh of the basic model.

generator that can meet these requirements, a mesh generator was implemented in MATLAB. The algorithm divided the sample into multiple, small sectors in which grid nodes were generated randomly around the pre-defined inclusions. Finally, Delaunay triangulation was performed on the entire collection of nodes (i.e., nodes that define the boundary of the inclusions as well as the randomly-generated nodes). The triangulation algorithm was based on the Quickhull algorithm for constructing convex hulls [20]. To keep calculation time in UDEC reasonable (about 15–24 h per model), the number of triangles was limited to approximately 8000. Of course, this limits the minimal representative length of the individual contacts of the discrete model and, consequently, the minimum fracture length that can be simulated [21]. The basic model consisted of about 12,200 contacts, and the average contact length was 3.0 mm. The quality of the generated mesh was dependent significantly on the choice of the input parameters, such as the minimum distance between grid nodes in relation to the dimensions of the sectors.

The first geometrical requirement of an appropriate mesh is that the boundary of the inclusions be respected by the edges of the generated triangles. (The edges are called 'elements' from now on.) Second, the distribution of the orientation of the elements should be as uniform as possible, as discussed in Section 2.2. Fig. 4a shows the distribution of the element orientation for the mesh of the basic model (Fig. 3b). The peaks at 0° and +90° are caused by the vertical and horizontal boundary nodes. Third, adjacent triangles should be of approximately the same size, and sharp triangles should be avoided to guarantee reasonable accuracy of the solution in UDEC. Quality parameters have been introduced to check the generated triangles [21]. The 'minimum triangle angle' is the smallest angle of the triangle. It is a measure to evaluate the skinniness of the triangles, and its aimed interval is [20°, 60°]. Another important parameter is the 'triangle aspect ratio', which is the ratio of the maximum edge size to the minimum altitude of the triangle. Its ideal interval is [1, 2.5]. The 'triangle quality' Q also is considered; it is the ratio of the smallest angle to the largest angle of the triangle. The ideal interval of Q is [0.4, 0.9]. Both the aspect ratio and Q values are indicative and not stringent. They serve as reference values when attempting to increase the quality of the mesh.

For the mesh of the basic model, only two minimum triangle angles were not situated in the desired interval of [20°, 60°] (Fig. 4b). Both triangles were adjacent to a pre-defined inclusion located near the boundary of the sample, and their minimum triangle angle was inherent to the pre-defined structure. Moreover, only 2.6% of the triangles had no aspect ratio in the interval of [1, 2.5] (Fig. 4c), and 21.6% of the triangles had triangle quality Q outside the range of [0.4, 0.9] (Fig. 4d). The latter was relatively high, but this was not necessarily a problem that affected the accuracy of the solution. After all, the interval was defined rather narrowly, and the quality parameters are only indicative and not stringent as mentioned before. Moreover, these triangles were distributed randomly through the sample mesh, and no clustering of the worse-shaped triangles was found.

3. Results

3.1. Influence of the volume percentage of inclusions

On the basis of the real 2D section and the basic model (Figs. 3a and b), 68 additional models were generated with 1, 5, 10, and 20 vol% of inclusions. For these models, the relative position of the inclusions and their shapes varied (e.g., explicitly rounded or sharp-ended), and the number of inclusions varied (e.g., one large, rounded inclusion as opposed to three smaller, rounded inclusions). This is illustrated by Table 3, which summarizes the number of models and inclusions for each considered volume percentage, and Fig. 5a–d, which show some examples of the modeled samples for 1, 5, 10 and 20 vol% of inclusions.

The evolution of the fracture pattern of the basic model (Fig. 3b) is presented in Figs. 6a–c for three different loading steps, as indicated on the stress–strain curve of Fig. 6d. The basic model has a UCS value of 4.4 MPa, while the UCS value of the homogeneous sample was 11.7 MPa. The nine inclusions (a total volume percentage of 10 vol%) reduced the strength by more than 60%. At relatively low vertical loads, a part of the material inside the inclusions started to fail. This is logical since the inclusions have lower strength properties. However, failure clearly was limited to specific parts of the inclusions. At a vertical load of 2.6 MPa, several vertical splitting types of fractures were induced in the matrix material at the top and at the bottom of the grouped inclusions (Fig. 6a). At higher vertical loads, especially after the UCS value had been reached (Fig. 6b), shear fractures also were induced. Finally, this resulted in a shear zone that extended from the upper left corner to the lower right corner of the sample (Fig. 6c). Fig. 6e presents three detailed fracture patterns of the tested samples, which were cored from a real soil-mix wall. The width of the pictures is about 30–50 mm. The soil inclusions and the induced fractures are clearly visible. Around the inclusions, there were always 1, 2, or 3 (locally) dominating fractures, both in the simulations and in the laboratory samples. For example, in the left picture, two fractures were induced at both extremities of the bottom part of the inclusion, which also were observed around several inclusions in the simulations. In the central and right pictures, fractures are observed somewhere along the middle of the inclusion or at the topmost or bottom points of the inclusion. Again,

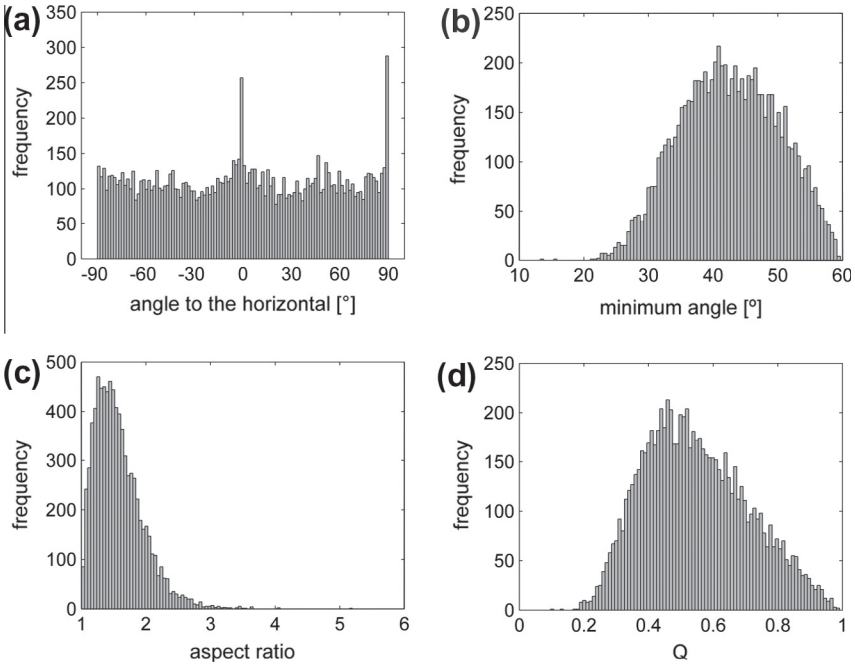

Fig. 4. Quality parameters for the mesh of the basic model. Distribution of (a) the element orientation, including orientation of boundary elements, (b) the minimum triangle angle, (c) the aspect ratio, and (d) the triangle quality *Q*.

Table 3
Overview of the number of models for the study of the effect of the volume percentage, shape, and number of inclusions.

vol%	# Models	# Inclusions
1	11	1, 2 or 3
5	18	1, 3, 4 or 6
10	30	1, 3, 9 or 10
20	10	1, 4, 12, 15 or 24

these fractures also were visible in the simulations. Finally, it is important to note that a larger numbers of cracks were observed at the upper left and lower right corner of the simulated sample in Fig. 6c. These cracks are part of the large-scale shear failure of the sample at the moment that UCS was reached and afterwards. These fractures are not visible on the detailed pictures of the laboratory samples (Fig. 6e).

Figs. 7a and b compare laboratory test data (strength and stiffness, respectively) of in situ cored samples from more than 10 different Belgian construction sites with the results of the numerical simulations. The mean and standard deviation are indicated for each dataset. As can be expected, the laboratory datasets and the results of the simulations were not exactly the same, but overall there was good agreement.

Both sets of results showed a similar downward trend in the volume percentage of the unmixed material. Generally, the simulated strength values were situated within the (wider) range of laboratory results (a total of 166 samples). This was less clear for the stiffness, although it was influenced by the lower number of available laboratory data (i.e., only 35 samples for all percentages of unmixed material). For 5%, 10% and 20%, only 4, 1, and 3 experimental data points, respectively, were available. The fact that the experimental data had a wider range is logical, because execution parameters (such as the amount of binder injected and the water/cement ratio of the binder) and soil types vary at different construction sites. This results in different strength and stiffness values, even if the samples were perfectly homogeneous [3]. So for a purely parametric study, numerical simulations are very suitable to study the effect of the volume percentage of inclusions on the strength and stiffness of a sample. First, the decrease of strength and stiffness was clearly larger than the percentage of inclusions in the sample. For a mere 1% of unmixed material, strength and stiffness were reduced, on average, by 13% and 3%, respectively. For 10% inclusions, on average, the strength was reduced by 50%, and the stiffness was reduced by 32%. Second, there is an overlapping zone between the strengths of 5% and 10% and 10% and 20%. This overlap was caused by the relatively large range for each volume percentage of inclusions. For stiffness, there was no overlap between successive volume percentages.

3.2. Influence of the shape, number and the relative position of the inclusions

The range of strength and stiffness for the same percentage of inclusions shows that parameters other than volume percentage are important, e.g., shape, number, and relative position of the

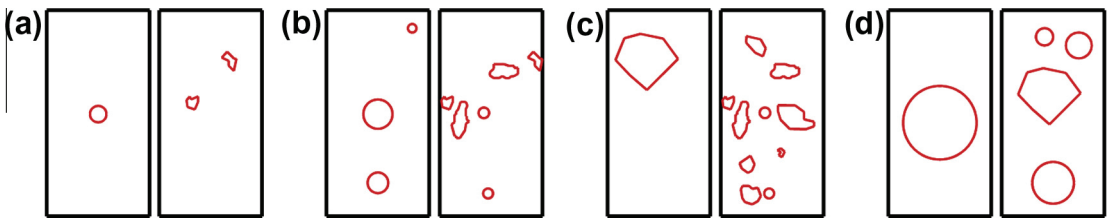

Fig. 5. (a–d) Overview of a number of models with 1%, 5%, 10%, and 20% of inclusions. The number of inclusions, their shapes, and their relative positions varied.

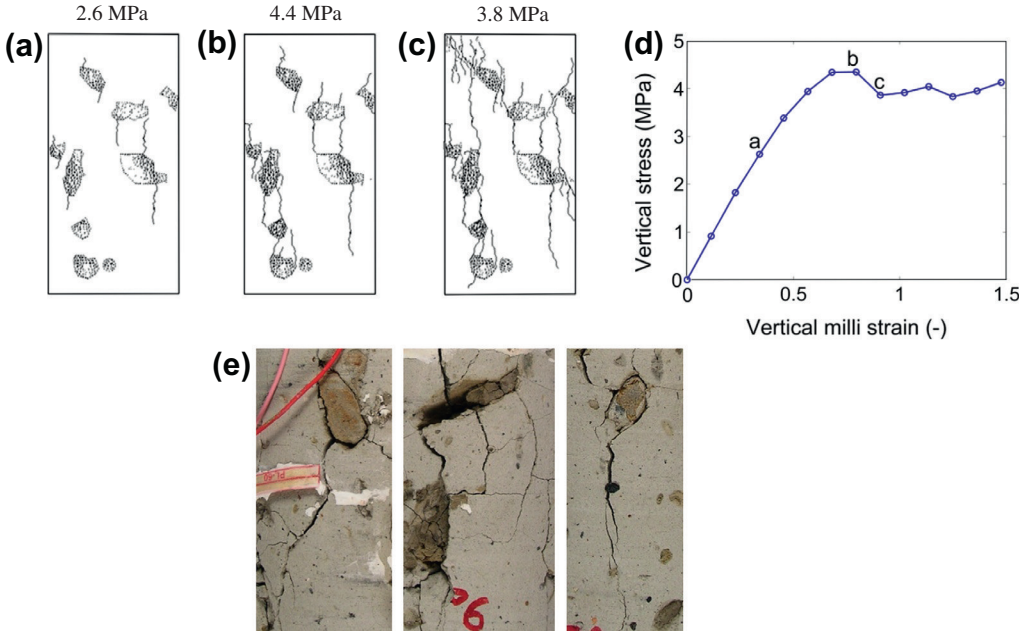

Fig. 6. (a–c) Evolution of the fracture pattern of the basic model. (d) Stress–strain curve of the basic model. (e) Examples of real fracture patterns of uniaxial loaded soil-mix cores (picture width is about 30–50 mm).

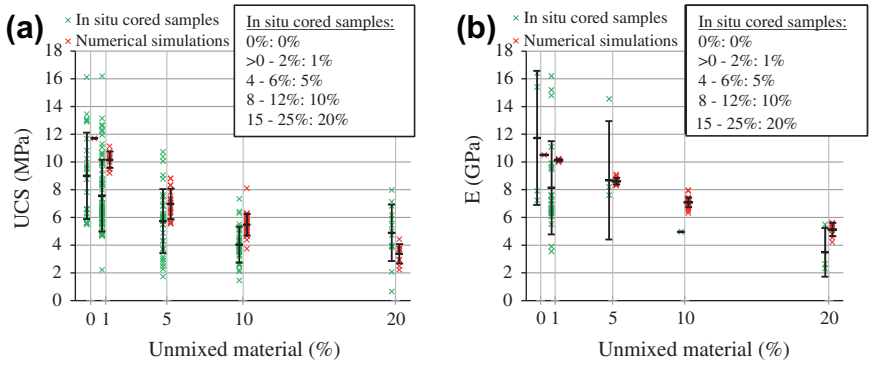

Fig. 7. Variation of (a) strength (UCS) and (b) stiffness (E) as a function of the volume percentage of unmixed material for the laboratory experiments on in situ cored samples [3] and the numerical simulations. The mean and standard deviation are indicated for each dataset.

inclusions. This hypothesis was confirmed by the 30 samples with 10% of inclusions, presented in Section 3.1 [5]. It was observed that strength and stiffness were reduced more by sharp-ended inclusions than by rounded inclusions, at least for the same number or size of inclusions. The strength of a sample also decreased significantly as the size of the inclusions increased, at least for the same shape and the same total percentage of inclusions (or in other words, a decrease in the number of inclusions per sample). To study the cause of the broad range of strength and stiffness for a given percentage of inclusions in more detail, 123 new models were generated.

The first 60 models contained the same three inclusions. One inclusion had a more rounded shape (4 vol%), while the other two inclusions (both 3 vol%) had horizontally elongated and vertically elongated shapes, respectively (Fig. 8a). For each of 10 different configurations of the inclusions (Fig. 8b), six models or permutations were generated. This means that, for 10 different relative positions, the centroids of the three inclusions were varied mutually. (For three inclusions, there were six models or permutations per position (Fig. 8c).) Apart from the influence of the relative position of the inclusions, these models also allowed us to study the influence of the shape of the inclusions for a given relative position.

Sixty-three additional models focused exclusively on how the relative positions of the inclusions influenced the strength and stiffness of a sample. As for the first 60 models, the total percentage of inclusions was 10 vol%. Now, five identical inclusions of 2 vol% were incorporated in the samples. The relative positions of the inclusions can be divided into six categories, as illustrated in Fig. 9. Within each category, the vertical and/or horizontal spacing between the inclusions was varied, as well as the global position of the configurations of the inclusions with respect to the borders of the sample.

Fig. 10 shows that the range of UCS values of all 123 models for the study of the relative position (3.1–9.2 MPa) was broader than the range of the models with 10% of inclusions for the study of the effect of the volume percentage (between 3.8 and 8.1 MPa, Fig. 7a). The range of Young's moduli of all 123 models (5–8.7 GPa) also was considerably larger than the range of the simulations for the study of the volume percentage (6.3 and 7.9 GPa, respectively, Fig. 7b). This is logical since the more simulations that are conducted, the greater the probability becomes that new

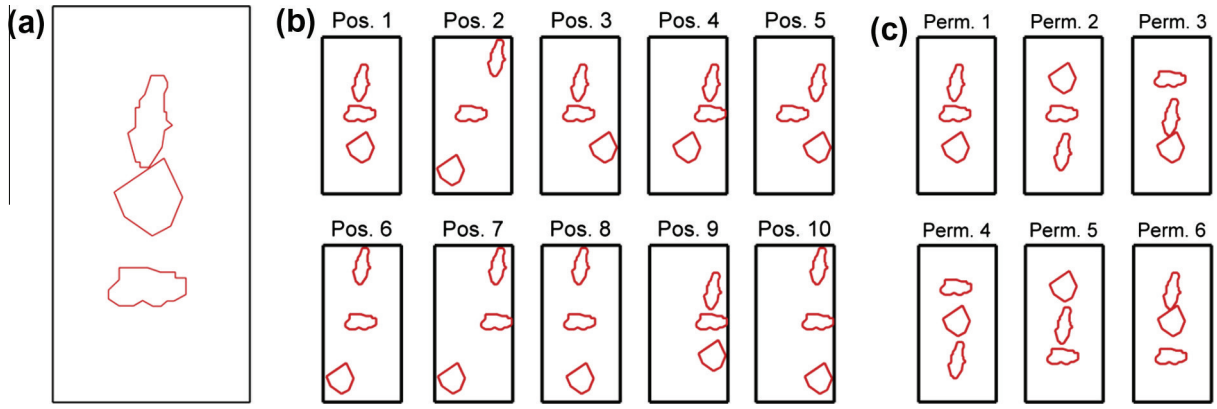

Fig. 8. (a) Three inclusions, each with a specific shape; (b) 10 models, each with a specific position of the three inclusions; and (c) six permutations of position 1.

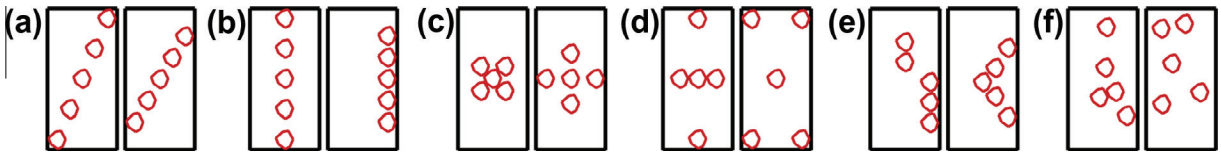

Fig. 9. Some examples of the six categories of inclusion configurations: (a) diagonally orientated (10 samples); (b) vertically aligned (10 samples); (c) grouped (10 samples); (d) widely spread (10 samples); (e) additional set (8 samples); and (f) randomly located (15 samples).

minimum and maximum values for strength and stiffness will be found. Moreover, the positioning of the inclusions was rather extreme in some cases (e.g., along the diagonal of the sample). Nevertheless, the conclusions drawn in Section 3.1 remain valid. Because of the wider range, the overlap of the strength between models with 5% and 20% of inclusions increased, and the stiffness values now overlap those of the models with 5% and 20% of inclusions. Finally, additional simulations did not change the conclusions about the good correspondence between the strength and stiffness values obtained from the simulations and from the laboratory results.

In further discussion, we no longer consider the simulations for the study of the effect of the volume percentage of inclusions. For the permutated models (Fig. 8), it was observed that the strength and stiffness values of each permutation position overlapped at least three other positions. The range within each permutation position was rather large, between 0.6 MPa (permutation position 2) and 2.2 MPa (permutation position 4) for the strength and between 0.2 GPa (permutation positions 1, 8, and 10) and 1.2 GPa (permutation position 7) for the stiffness. Thus, the influence of the shape of the inclusions cannot be neglected, particularly not for the strength. The influence of the shape on the Young's modulus was less pronounced if the inclusions were aligned vertically. (Note that this was not observed for the strength.) For the 63 models with five identical inclusions (Fig. 9), the strength values varied between 1.4 MPa (configuration b) and 3.7 MPa (configuration a). The stiffness values ranged from 0.5 GPa (configuration b) to 3.2 GPa (configuration a). The simulations clearly demonstrated the influence of the relative position of the inclusions on the strength and stiffness of a sample.

First, it was observed that strength and stiffness decreased if the inclusions were located along the diagonal of the sample (instead of along a vertical line). This was shown clearly by the higher strength and stiffness values for permutation positions 1, 8, 9, and 10 (on average, 7.6 MPa and 7.9 GPa, respectively, Fig. 10a) and for configuration b (on average, 8.6 MPa and 8.6 GPa, respectively, Fig. 10b). Inclusions along the diagonal probably facilitated a global shear failure. Moreover, the width of the vertical zones without inclusions was larger when the inclusions were aligned vertically, clearly affecting strength and stiffness. Fig. 11a and b, respectively, present the relationships between strength and stiffness and the ratio $w_{i/t}$ of the total width of inclusions, i, to the sample width, t (as illustrated in Fig. 11c). It was confirmed that both parameters strongly depend on this ratio. Moreover, a general negative trend between strength and stiffness and the ratio $w_{i/t}$ clearly was observed. In Section 3.3, these observations were linked to the fracture patterns that were observed. However, a significant overlap also was observed, e.g., the largest UCS value for a width ratio of 60% was still larger than the smallest value for the 20% ratio. The overlap probably was even larger for stiffness. These overlaps can be explained in part by the influence on strength and stiffness of volume percentage of inclusions, the shape of the inclusions, and the number of inclusions. However, other parameters that describe the relative position of the inclusions also have some influence.

Second, strength and stiffness also decreased if the vertical distance between the inclusions decreased, since inclusions tend to act as one large inclusion. However, the influence was smaller than that of the vertical alignment of the inclusions. Note that this effect cannot be derived from Figs. 10a and b, since they concern models within the same category.

Third, stiffness also decreased if the inclusions were located closer to the border of the sample. For strength, this could not be concluded unambiguously. The effect of the upper and lower borders on strength and stiffness was more difficult to describe with the available simulations. Probably, there were too many interfering effects, such as the relative position of the inclusions, the distance to the horizontal and/or vertical borders, and the concentration and shape of the inclusions.

A final interesting observation was that, for the 15 models with randomly-located inclusions, the values of strength (4.2–5.9 MPa) and stiffness (6.3–7.8 GPa) were situated between the extremes of all of the simulations with 10% inclusions. However, the values were less extreme than those that corresponded to inclusions that were perfectly aligned vertically and inclusions that were

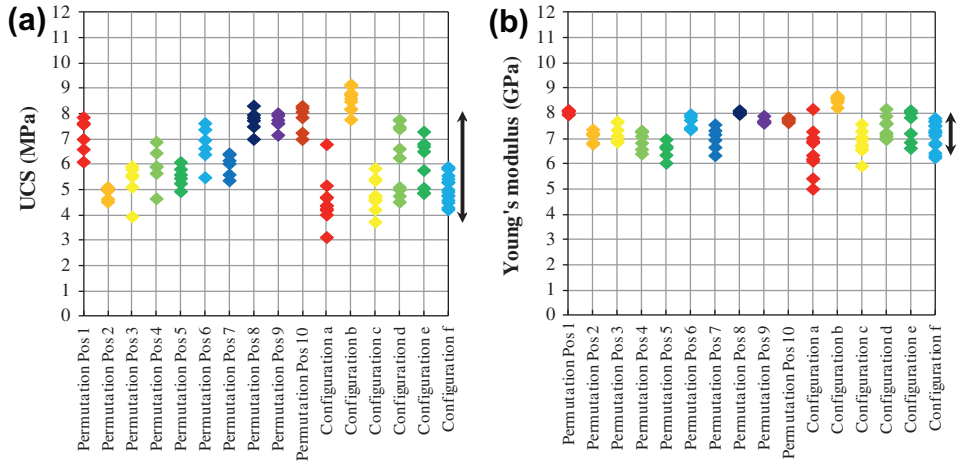

Fig. 10. Comparison of (a) UCS values and (b) Young's moduli of all 123 models for the study of the influence of the relative position of the inclusions. The arrows on the right side of both figures indicate the range of the models described in Section 3.1 with 10% of inclusions.

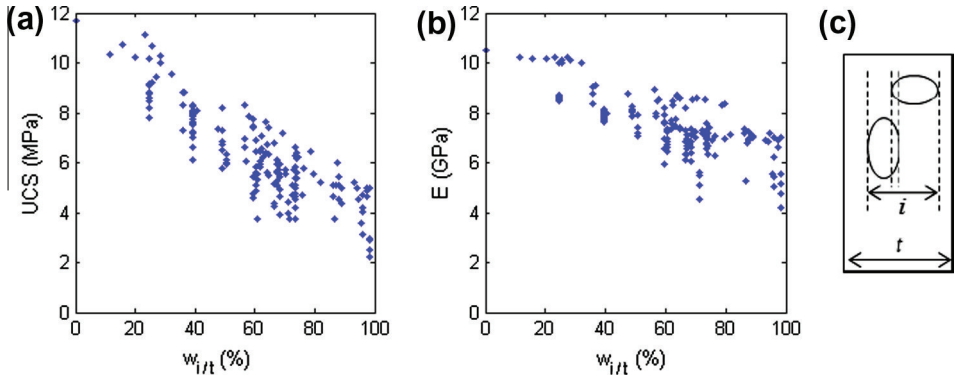

Fig. 11. (a and b) Relation between the strength and the stiffness, respectively, and the ratio $w_{i/t}$. (c) Illustration of the definition of the ratio $w_{i/t} = i/t$.

positioned diagonally. By way of comparison, the range of all strength and stiffness values of models with 10% inclusions was 3.1–9.1 MPa and 5.0–8.7 GPa, respectively.

3.3. Relation with fracture pattern

The fracture patterns in most samples were quite similar (Fig. 12a–d). At relative low stress levels (less than 50% of the strength), vertical-extension fractures were initiated at the lower and upper parts of the inclusions. (Also, see Fig. 6a–c for the evolution of the fracture pattern of the basic model.) Shear fractures were observed at the sides of the inclusions only at stress levels near the UCS value of the sample, after which the sample finally failed due to a combination of shear and extension fractures.

A similar fracture pattern was observed during laboratory UCS tests of soil-mix samples. This was already illustrated in Fig. 6e and in Fig. 13, which shows the evolution of the fracture pattern of a real soil-mix sample during a UCS test. The sample had a diameter and height of 110 and 220 mm, respectively, and it was quite homogeneous. However, a soil inclusion with a diameter of 20–30 mm embedded in a larger, weaker zone was clearly visible. During loading, a shear fracture developed in the left (homogeneous) part of the sample, and vertical cracks were initiated at the top and bottom of the inclusion. The final failure mode of the sample was a combination of vertical-extension fractures and shear fractures.

Most of the effects of inclusions, as described in this article, can be explained by the observed fracture patterns. For example, stress peaks near sharp-ended inclusions are greater than those that were close to rounded inclusions, which makes fractures initiate at lower stress levels and leads to lower strength and stiffness. (Compare Figs. 12a and c.) Fracturing also was initiated at lower stress levels when one large inclusion was present instead of three smaller inclusions, at least if these three inclusions were aligned vertically. (Compare Figs. 12a, b, and d.) Again, this was caused by higher stress peaks near the largest inclusions (i.e., because a higher horizontal distance must be bridged). However, the fact that the three inclusions were aligned vertically also was very important. To illustrate this, Fig. 12d shows the fracture pattern of a sample with the same three inclusions, which are now positioned diagonally. This sample had about the same strength and stiffness as the sample with one large, rounded inclusion. The large reduction of strength in comparison to the model with three vertically-aligned inclusions was caused by the diagonal orientation of the inclusions. Thus, the width of the vertical zones without inclusions was smaller, and the inclusions did not protect each other. Moreover, the stress peaks around the stress-relieved zones interfered with and probably amplified each other.

Finally, if the vertical spacing between the inclusions of Fig. 12b was decreased, the inclusions tended to form one larger inclusion. Overlapping zones with increased stresses expanded again and the amplifying effect increased. This caused earlier initiation of fractures (at lower vertical loads), but the vertical-extension fractures around the central inclusion also reached the upper and lower inclusions more rapidly. Thus, the distance traveled through the stronger material before reaching other weak inclusions was

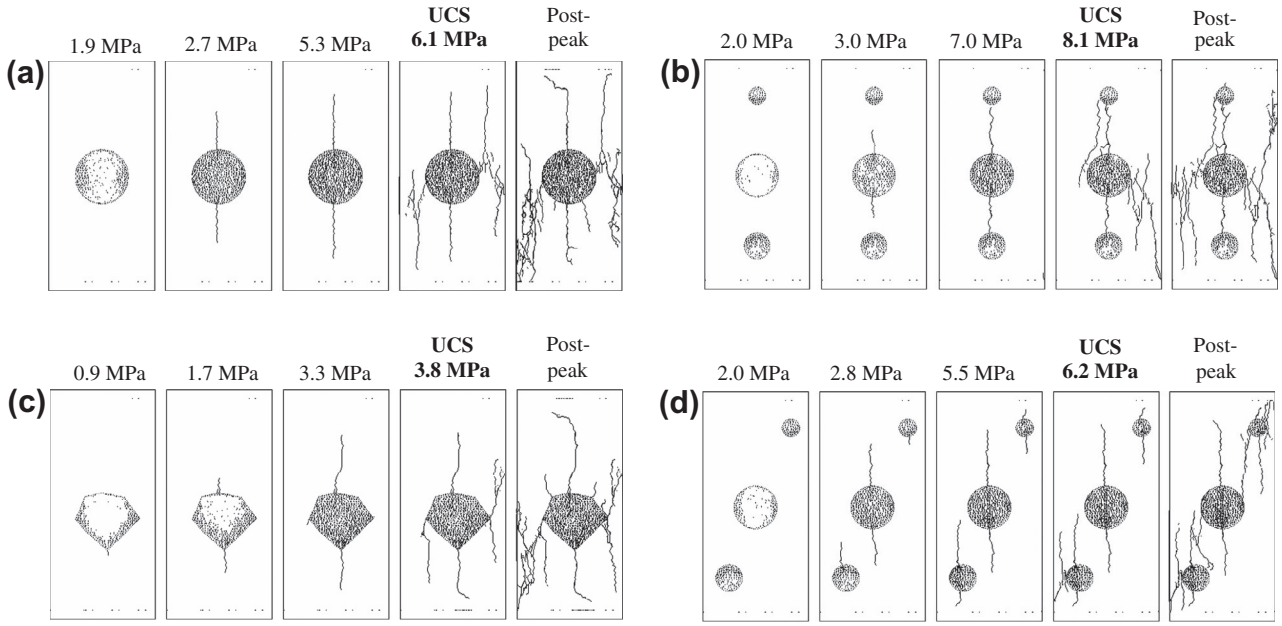

Fig. 12. Illustration of the fracture pattern at successive loading steps of four samples of the original set, each with 10% of inclusions; the shape and number of inclusions were different. The corresponding stiffness values for the four models (a–d) were 7.2, 8.0, 6.7, and 7.4 GPa, respectively.

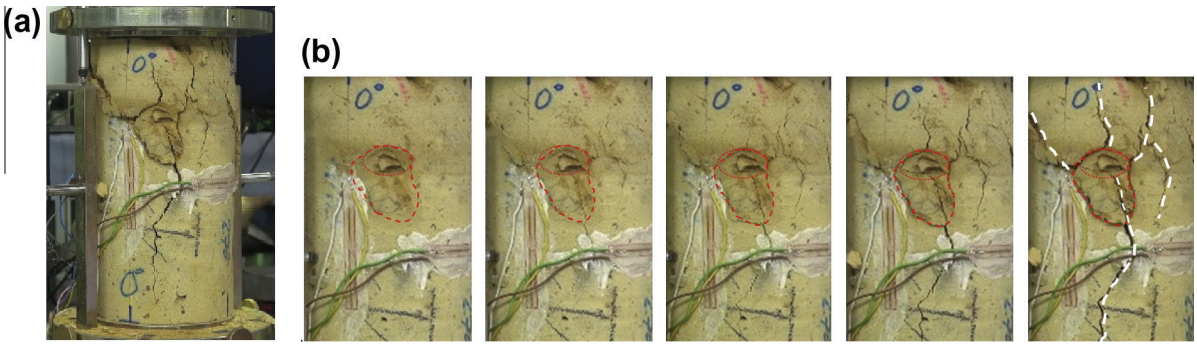

Fig. 13. (a) Picture of the final fracture pattern for the entire soil-mix sample after a UCS test. (b) Evolution of fracture pattern around the largest soft inclusion in successive loading steps.

decreased. Because propagation through these inclusions occurs much faster, a much larger part of the sample was harmed. Again, this results in lower strength and stiffness.

4. Conclusions and future work

Although calibration of the numerical discrete model was a time-consuming process, the results showed that numerical simulations can be very beneficial for performing sensitivity analyses relatively easily and for acquiring a better understanding of the effect of soft inclusions on the behavior of real samples. The influence of soil inclusions on the strength and stiffness of soil-mix material was investigated by three sets of simulations (a total of 192 simulations). It was observed that soft inclusions have a large impact on the strength and stiffness of a sample. Moreover, there was a good correlation between the numerical simulations and laboratory test results. However, the simulations showed that the volume percentage of the inclusions, their relative positions, and their shapes and numbers all influenced the strength and stiffness. It was demonstrated that UDEC is suitable for the simulation of fracture initiation and growth in soil-mix material with soft inclusions. The simulated fracture patterns were comparable to those observed in real soil-mix samples that were loaded uniaxially.

Apart from the simulations of UCS tests on samples, simulations of other test configurations, such as bending tests or compression tests on large scale samples, would be interesting and beneficial. As part of the IWT project on soil-mix material, several large-scale UCS tests on soil-mix blocks (600×1200 mm) have been conducted, and the results will be compared with the UCS values of the samples (100×200 mm) of the same material. In this way, the aim is to obtain a better understanding of the scale effect. Moreover, the laboratory tests conducted so far show that the strength of the soil-mix blocks was about 30–50% less than the strength of the core samples [4].

Acknowledgments

This project was made possible by the financial support of the Flemish government agency for Innovation by Science and Technology (IWT). It was the result of cooperation between the Belgian Building Research Institute (BBRI), the Belgian Association of Foundation Contractors (ABEF), and KU Leuven. Special thanks go to Flor De Cock, Nicolas Denies, and Bart Lameire.

References

[1] Ganne P, Huybrechts N, De Cock F, Lameire B, Maertens J. Soil mix walls as retaining structures – critical analysis of the material design parameters. In: Proceedings of the international conference on geotechnical challenges in megacities, Moscow; 2010. p. 991–8.

[2] Ganne P, Denies N, Huybrechts N, Vervoort A, Tavallali A, Maertens J, et al. Soil mix: influence of soil inclusions on the structural behavior. In: Proceedings of the 15th European conference on soil mechanics and geotechnical engineering, Athens; 2011. p. 977–82.

[3] Denies N, Huybrechts N, De Cock F, Lameire B, Vervoort A, Van Lysebetten G, et al. Soil mix walls as retaining structures – mechanical characterization. In: Proceedings of the TC 211 international symposium on ground improvement, vol. 3, Brussels; 2012. p. 99–115.

[4] Vervoort A, Tavallali A, Van Lysebetten G, Maertens J, Denies N, Huybrechts N, et al. Mechanical characterization of large scale soil mix samples and the analysis of the influence of soil inclusions. In: Proceedings of the TC 211 international symposium on ground improvement, vol. 3, Brussels; 2012. p. 127–36.

[5] Vervoort A, Van Lysebetten G, Tavallali A. Numerical modeling of fracturing around soft inclusions. In: Proceedings of the southern hemisphere international rock mechanics symposium, Sun City, South-Africa; 2012. p. 33–46.

[6] Kolari K. Damage mechanics model for brittle failure of transversely isotropic solids. Finite element implementation, Ph.D. dissertation, VTT Publications 628, Espoo, Finland; 2007. 195p.

[7] Oliver J, Huespe AE. Continuum approach to material failure in strong discontinuity settings. Comput Meth Appl Mech Eng 2004;193:3195–220.

[8] Bouchard PO, Bay F, Chastel Y. Numerical modeling of crack propagation: automatic remeshing and comparison of different criteria. Comput Meth Appl Mech Eng 2003;192:3887–908.

[9] Belytschko T, Lu YY, Gu L. Element-free Galerkin methods. Int J Numer Meth Eng 1994;37:229–56.

[10] Rabczuk T, Belytschko T. Cracking particles: a simplified mesh free method for arbitrary evolving cracks. Int J Numer Meth Eng 2004;61(13):2316–43.

[11] Belytschko T, Black T. Elastic crack growth in finite elements with minimal remeshing. Int J Numer Meth Eng 1999;45(5):601–20.

[12] O'Sullivan C. Particulate discrete element modeling, a geomechanics perspective. London (United Kingdom): Spon Press, Taylor & Francis; 2011. 561p.

[13] Potyondy DO, Cundall PA. A bonded-particle model for rock. Int J Rock Mech Miner Sci 2004;41(8):1329–64.

[14] Itasca. UDEC v4.0 manual. Itasca Consulting Group Inc., Minnesota, USA; 2004.

[15] Debecker B, Vervoort A. A detailed 2D study of the fracture behavior of slate through discrete simulations following laboratory experiments. Int J Rock Mech Miner Sci 2013;61:161–70.

[16] Tempone P, Lavrov A. DEM modeling of mudlosses into single fractures and fracture networks. In: Proceedings of the 12th international conference of the international association for computer methods and advances in geomechanics, Goa, India; 2008. p. 2475–82.

[17] Cundall PA. A computer model for simulating progressive large scale movements in block rock systems. In: Proceedings of the international society for rock mechanics symposium, vol. 1, Nancy, France; 1971, paper II-8.

[18] Cundall PA, Board M. A microcomputer program for modeling large-strain plasticity problems. In: Proceedings of the 6th international conference on numerical methods in geomechanics, Rotterdam; 1988. p. 2101–8.

[19] Debecker B, Vervoort A, Napier JAL. Fracturing in and around a natural discontinuity in rock: a comparison between boundary and discrete element models. In: Proceedings of the 5th international conference on engineering computational technology, Las Palmas de Gran Canaria; 2006, paper 168.

[20] Barber CB, Dobkin DP, Huhdanpaa H. The quickhull algorithm for convex hulls. ACM Trans Math Softw 1996;22(4):469–83.

[21] Debecker B, Vervoort A. A 2D triangular Delaunay grid generator for the simulation of rock features. In: Proceedings of the 5th international conference on engineering computational technology, Las Palmas de Gran Canaria; 2006, paper 220.